Research Article | Vol. 29, No. 14 / 5 July 2021 / Optics Express 21300

Optics EXPRESS

Anomalous spatial coherence changes in radiation and scattering

S. A. Wadood,[1,2] H. F. Schouten,[3] D. G. Fischer,[4] T. D. Visser,[1,3,5] and A. N. Vamivakas[1,2,6,7,*]

[1] The Institute of Optics, University of Rochester, Rochester, New York 14627, USA
[2] Center for Coherence and Quantum Optics, University of Rochester, Rochester, New York 14627, USA
[3] Department of Physics and Astronomy, Vrije Universiteit, Amsterdam 1013LP, The Netherlands
[4] Research and Engineering Directorate, NASA Glenn Research Center, Cleveland, OH 44135, USA
[5] School of Physics and Electronics, Shandong Normal University, Jinan 250014, China
[6] Department of Physics and Astronomy, University of Rochester, Rochester, New York 14627, USA
[7] Materials Science, University of Rochester, Rochester, NY 14627, USA
[*] nick.vamivakas@rochester.edu

Abstract: The superposition of two partially correlated waves is shown to produce fields with drastically altered coherence properties. It is demonstrated, both theoretically and experimentally, that two strongly correlated sources may generate a field with practically zero correlation between certain pairs of points. This anomalous change in coherence is a general phenomenon that takes place in all cases of wave superposition, including Mie scattering, as is shown. Our results are particularly relevant to applications in which it is assumed that highly coherent radiation maintains its spatial coherence on propagation, such as optical systems design and the imaging of extended sources.

1. Introduction

The coherence properties of a wavefield determine its evolution in space and time and its interaction with material structures. The temporal coherence of an emitted wavefield is primarily determined by the bandwidth of the source, whereas its spatial coherence is determined by the relative size of its coherence area to its physical extent. These two forms are typically coupled, although a monochromatic field can be spatially partially coherent when the source is composed of (spectrally filtered) independent emitters. It is well known that the spatial coherence of a partially coherent wavefield can change on propagation [1]. For example, according to the van Cittert-Zernike theorem, the field radiated by a completely uncorrelated source becomes highly correlated in the far zone [2]. This explains why sunlight can produce interference fringes on earth [3–5]. Likewise, the field radiated by the broad class of Gaussian Schell-model sources becomes more coherent on propagation (see Eq. (5.6–107) of Ref. [2]). Less well-known is the fact that partially coherent sources can generate fields with increased spatial coherence for certain pairs of points and decreased (even zero) coherence for others [6]. Here, we report practically fully coherent sources that generate fields with zero coherence for certain pairs of points. Further, we suggest that this phenomenon is a general manifestation of wave interference and is also observed in the scattering of almost fully coherent light from dielectric spheres.

The extreme reduction in coherence is demonstrated for the two cases of (1) the field generated by two correlated point sources and (2) the field generated by scattering of (practically) coherent light on a dielectric sphere, and is validated experimentally for the case of correlated point sources. To the best of our knowledge, a strong reduction in coherence has not been demonstrated before for free-space propagation of radiated or scattered fields.

#428108 https://doi.org/10.1364/OE.428108
Journal © 2021 Received 19 Apr 2021; revised 10 Jun 2021; accepted 11 Jun 2021; published 22 Jun 2021

Optics EXPRESS

2. Radiation

Consider two partially correlated scalar point sources located at points Q_1 and Q_2 in the plane $z = 0$, separated by a distance d along the x axis (see Fig. 1). We analyze the superposition of their fields along the x axis in the plane $z = z_0$. The field at an observation point P_1 equals

$$U(P_1, \omega) = U(Q_1, \omega)\frac{e^{iknR_{11}}}{R_{11}} + U(Q_2, \omega)\frac{e^{iknR_{21}}}{R_{21}}, \tag{1}$$

where $U(Q_i, \omega)$ denotes the field at Q_i at frequency ω, with $i = 1, 2$. Furthermore, k is the free-space wavenumber, n is the refractive index of the background medium, and R_{ij} is the distance Q_iP_j, for $i, j = 1, 2$. The coherence of the field in the plane $z = z_0$ is characterized by the cross-spectral density (CSD) function, which is defined as $W(P_1, P_2, \omega) \equiv \langle U^*(P_1, \omega)U(P_2, \omega)\rangle$, with the angular brackets denoting an ensemble average. The spectral density is given by $S(P_1, \omega) \equiv \langle |U(P_1, \omega)|^2\rangle$, namely,

$$S(P_1, \omega) = \frac{S_1(\omega)}{R_{11}^2} + \frac{S_2(\omega)}{R_{21}^2} + \frac{2\sqrt{S_1(\omega)S_2(\omega)}}{R_{11}R_{21}}\mathrm{Re}\left[\mu_{12}(\omega)e^{ikn(R_{21}-R_{11})}\right]. \tag{2}$$

Here $S_i(\omega) = \langle |U(Q_i, \omega)|^2\rangle$ is the spectral density of source Q_i, and the spectral degree of coherence of the two sources is defined as

$$\mu_{12}(\omega) \equiv \frac{\langle U^*(Q_1, \omega)U(Q_2, \omega)\rangle}{\sqrt{S_1(\omega)S_2(\omega)}} = \frac{W(Q_1, Q_2, \omega)}{\sqrt{S_1(\omega)S_2(\omega)}}. \tag{3}$$

It can be shown [2] that $0 \le |\mu_{12}(\omega)| \le 1$. The lower bound corresponds to the complete absence of coherence, whereas the upper bound describes a fully coherent field. For all intermediate values the field is said to be partially coherent. The spectral degree of coherence at P_1 and P_2 is

$$\begin{aligned}\mu(P_1, P_2) = \Bigg[& S_1\frac{e^{ikn(R_{12}-R_{11})}}{R_{11}R_{12}} + \langle U^*(Q_1)U(Q_2)\rangle\frac{e^{ikn(R_{22}-R_{11})}}{R_{11}R_{22}} \\ & + S_2\frac{e^{ikn(R_{22}-R_{21})}}{R_{22}R_{21}} + \langle U^*(Q_2)U(Q_1)\rangle\frac{e^{ikn(R_{12}-R_{21})}}{R_{12}R_{21}}\Bigg] \\ & \times [S(P_1)S(P_2)]^{-1/2},\end{aligned} \tag{4}$$

where from now on we omit the ω dependence.

To illustrate the decrease of coherence we consider the case that the spectral densities of the two sources are equal, i.e., $S_1 = S_2 = S$. Furthermore, we take μ_{12} to be real and positive, and set the refractive index $n = 1$. It then follows (see Appendix, Sec. A) that in the far zone the spectral degree of coherence in the angular directions zero and θ_1 equals, to a good approximation,

$$|\mu(\theta_1, 0)|^2 = \frac{(1 + \mu_{12})\cos^2[k(d/2)\sin\theta_1]}{1 + \mu_{12}\cos(kd\sin\theta_1)}. \tag{5}$$

Due to the presence of the cosine term in the numerator, Eq. (5) has the surprising implication that no matter how strong the two point sources are correlated, there will be certain directions θ_1 for which $\mu(\theta_1, 0) = 0$ (provided the separation d between the two sources is at least several wavelengths and $\mu_{12}<1$). In other words, we find that even for two almost perfectly coherent point sources, there are always pairs of directions in which their combined field is completely uncorrelated. An example is given in Fig. 2. It is seen that the approximation (5) is in excellent agreement with the exact result (4). The angular regions in which the far-zone coherence is increased (i.e., $|\mu(\theta_1, 0)|>\mu_{12} = 0.85$) are interspersed with regions in which the spectral degree

Optics EXPRESS

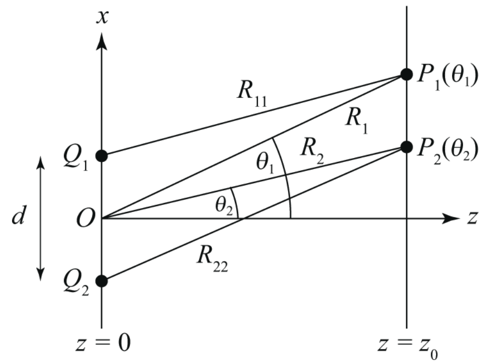

Fig. 1. The superposition of the fields radiated by Q_1 and Q_2 is observed at $P_1(\theta_1)$ and $P_2(\theta_2)$. The four distances are $R_{11} = Q_1P_1$, $R_1 = OP_1$, $R_{22} = Q_2P_2$, and $R_2 = OP_2$; R_{12} and R_{21} are not shown.

of coherence is strongly reduced, and even reaches zero. The spectral density, given by Eq. (19) in the Appendix Sec. A,

$$S(\theta_1) = \frac{2S}{R^2}\left[1 + \mu_{12}\cos(kd\sin\theta_1)\right], \tag{6}$$

is also plotted (solid green curve). It follows from this expression that the minima of $S(\theta_1)$ coincide with those of $|\mu_{12}(\theta_1, 0)|$. We emphasize that the strong reduction of coherence is not a far-zone effect. The choice of far-zone fields as an illustration is motivated by the fact that for those cases simple analytical results like Eq. (5) can be derived. For observation points much closer to the source plane (e.g., $z_0 = 200\,\lambda$) a numerical evaluation of Eq. (4) yields the blue curve 4. A decrease of $|\mu_{12}(\theta_1, 0)|$ to near-zero values is again observed, but now at shifted angles. The behavior in the limits of complete incoherence ($\mu_{12} = 0$) and full coherence ($\mu_{12} = 1$) is as expected, and is described in Appendix Sec. B. A suggestive explanation for this phenomenon is discussed at the end of Sec. 4.

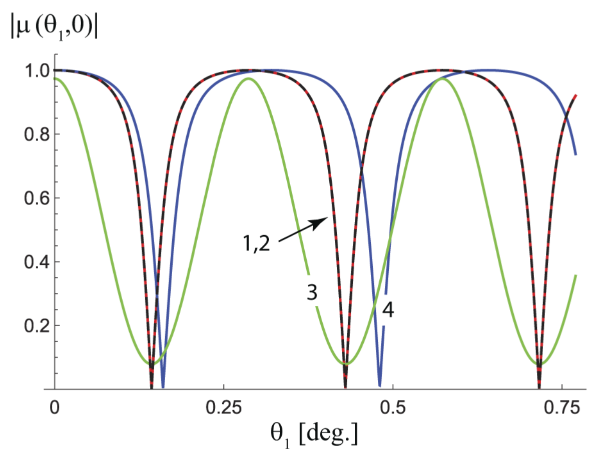

Fig. 2. Modulus of the spectral degree of coherence $\mu(\theta_1, 0)$. The red-black curve [1,2] represents both the exact expression (4), and the approximation given by Eq. (5). The green curve [3] is the scaled spectral density $S(\theta_1)$. In this example $S_1 = S_2$, $d = 200\,\lambda$, $z_0 = 10^4\,\lambda$, $n = 1$, and $\mu_{12} = 0.85$. The blue curve [4] is $|\mu(\theta_1, 0)|$ for the case $z_0 = 200\,\lambda$.

Optics EXPRESS

Three contour plots of $|\mu(\theta_1, \theta_2)|$, calculated from Eq. (4) (i.e., without use of any approximations), are shown in the top row of Fig. 3. All plots are restricted to a representative 2D angular interval. Panel a) is for the case $\mu_{12} = 0.94$. The spectral degree of coherence of the far-zone field exhibits a more or less square pattern. The case of a pair of point sources that are somewhat less correlated, with $\mu_{12} = 0.75$, is shown in b). The pattern is seen to become more sinuous, and gradually transitions to a purely diagonal form as presented in c). This represents two virtually uncorrelated point sources with $\mu_{12} = 1.0 \times 10^{-22}$. We notice that in all three cases the spectral degree of coherence ranges from near-zero values to unity. The increase of coherence in panel c) is consistent with the van Cittert-Zernike theorem. However, to the best of our knowledge, the anomalous decrease of coherence in the far-zone field of two strongly correlated sources as shown in panels a) and b) has not been reported before.

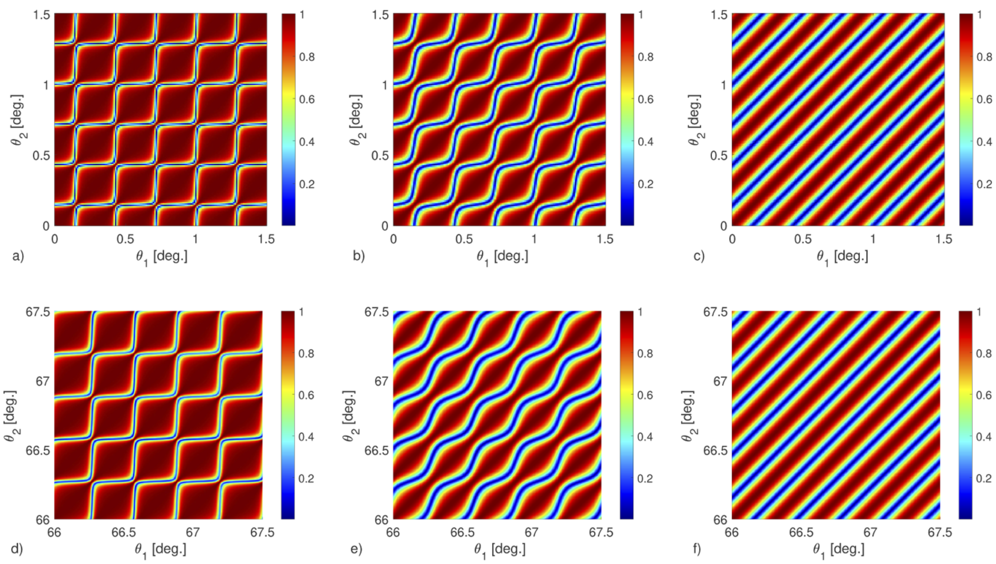

Fig. 3. Contours of $|\mu(\theta_1, \theta_2)|$, the modulus of the spectral degree of coherence as a function of θ_1 and θ_2. The top row is for the far-zone field generated by two partially correlated point sources for three values of μ_{12}. a) $\mu_{12} = 0.94$, b) $\mu_{12} = 0.75$, c) $\mu_{12} = 1.0 \times 10^{-22}$. The other parameters are as in Fig. 2. The bottom row is for the far-zone field scattered by a dielectric sphere of radius $a = 100\lambda$. From left to right the coherence radius of the incident field decreases from $\sigma = 500\lambda = 5a$, to $\sigma = 150\lambda = 1.5a$, to $\sigma = 20\lambda = 0.2a$.

3. Experimental verification

A partially coherent field can be synthesized as an incoherent superposition of fully coherent modes via the coherent mode decomposition (CMD) [7]. In the CMD, a given field realization is represented as $U(\mathbf{r}) = \sum_m a_m \phi_m(\mathbf{r})$, where the random expansion coefficients a_m are uncorrelated, i.e., $\langle a_m^* a_n \rangle = \lambda_m \delta_{mn}$ with $\lambda_m > 0$, and the field modes ϕ_m are orthonormal. It follows then that the cross-spectral density takes the form

$$W(\mathbf{r}_1, \mathbf{r}_2) = \sum_m \lambda_m \phi_m^*(\mathbf{r}_1) \phi_m(\mathbf{r}_2). \tag{7}$$

In our case, the field to be synthesized is a secondary source consisting of a pair of partially correlated point sources, which can be approximated mathematically as $U(x, y) = A_1 \delta^{(2)}(x + d/2, y) + A_2 \delta^{(2)}(x - d/2, y)$, where we take $\langle |A_1|^2 \rangle = \langle |A_2|^2 \rangle = 1$ and $\mu_{12} = \langle A_1^* A_2 \rangle$ is their spectral degree of coherence. We utilize a two-dimensional geometry for simplicity. It can be shown (see Appendix Sec. C) that the CMD of this source distribution contains only two coherent modes, which correspond to symmetric and anti-symmetric combinations of the two point sources. It can also be shown that their correlation is

$$\mu_{12} = (\lambda_1 - \lambda_2)/(\lambda_1 + \lambda_2). \tag{8}$$

The field produced by each source coherent mode in the far-zone (or interference region) is realized, not by actual propagation into the far-zone, but by the Fourier transformation operation of a (FT) lens. As illustrated in the Appendix Sec. D, the far-zone forms of the two coherent modes in the back focal plane of the FT lens are a cosine and a sine, respectively [8, Ch. 5].

The utility of the CMD, as embodied by Eq. (7), is that the contribution of each coherent mode to the cross-spectral density can be generated and measured independently, and then the individual contributions can be summed incoherently with an appropriate weighting [9,10]. In our case the contributions of each mode were recorded individually and summed numerically, thus creating *in silico* the far-zone CSD of a source with a prescribed value of μ_{12}. This would be hard to achieve with traditional methods using diffusers.

Measurement of the cross-spectral density (and ultimately the degree of spectral correlation) is performed using a Michelson-type interferometer, in which the output intensity for each coherent mode (which contains an interference term proportional to the degree of coherence) is individually recorded on a CCD.

Referring to Fig. 4, we see that the coherent modes in the plane $z = 0$ (secondary source plane) are generated by laser illumination of a Spatial Light Modulator (SLM) programmed with one of two specific phase profiles. Upon illumination with a flat-phase broad Gaussian beam, the first order diffracted light ($p = 1$) from the phase grating contains the desired coherent mode in the Fourier plane at $z = 0$. The required phase grating on the SLM that generates the coherent modes was found by an inverse method explained in [11]. The laser was power-stablized and the interferometer path-stabilized to keep the phase difference constant during the measurement. After spatially filtering the $p = 1$ order, the coherent mode is propagated to the far-zone using another FT lens and then presented to the input of the interferometer at $z = 2f$. The interferometer's top arm is a $2f$ imaging system consisting of a concave mirror and an SLM (not shown) to implement a quadratic phase to cancel the defocus due to diffraction. This arm realizes the transformation $x \longrightarrow -x$. The horizontal arm contains a $4f$ system which images the field with unit magnification, after two reflections. Experimental details of the interferometer are described in [12]. Its output field is

$$U_{\mathrm{out}}(x, z = 2f) \propto \phi_i(x, z = 2f) + e^{i\theta}\phi_i(-x, z = 2f), \quad (i = 1, 2) \tag{9}$$

where θ is the global phase difference between the two arms. For $i = 1$ and $\theta = 0$ we observe the even mode at the output. For $i = 2$ and $\theta = \pi$ the odd mode is observed. At any given time only one of the two coherent modes is sent through the setup, and the recorded intensities are added in software. Care was taken to equalize the total power in the two coherent modes. A total of 20 intensity frames was recorded by the CCD for both modes. By digitally adding, for example, all twenty frames of mode ϕ_1 with a single frame of mode ϕ_2, we have set $\lambda_1 = 20$ and $\lambda_2 = 1$. Inserting these values into Eq. (8) it is seen that we have then created the case for which the spectral degree of coherence has the value

$$\mu_{12} = \frac{20 - 1}{20 + 1} = 0.904. \tag{10}$$

By gradually adding more frames of mode ϕ_2 to the sum of the all recorded frames of ϕ_1 we get progressively lower values of μ_{12}.

An example of the data that were produced for the case $\mu_{12} = 0.904$ is shown in Fig. 5. To obtain $W(x, -x)$ we have subtracted the individual spectral densities $W(x, x)$ of each interferometer

Optics EXPRESS

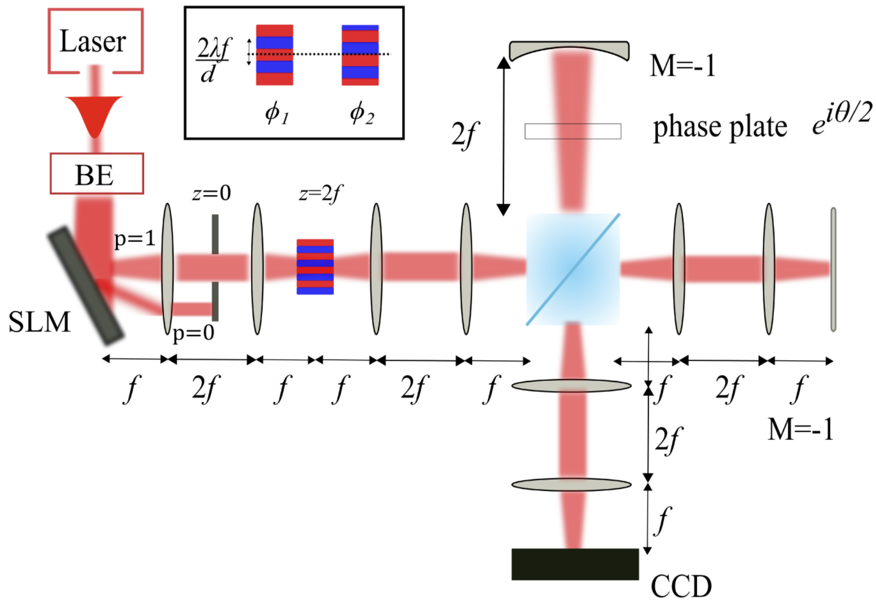

Fig. 4. Experimental setup. A 795 nm Gaussian beam passes through a beam expander (BE) and is then converted into either a symmetric (ϕ_1) or an antisymmetric (ϕ_2) coherent mode, shown in the inset, via a mode converter consisting of a phase SLM and a spatial filtering setup, which selects the $p = 1$ diffraction order. Polarization optics and attenuators, not shown, are used to control the power of the beam.

arm, obtained by blocking the other arm, from the combined image when both arms are not blocked. The result is an image that is proportional to $W(x, -x) = \langle U^*(x)U(-x)\rangle$. Each row in Fig. 5 represents a time averaged realization of $U^*(x)U(-x)$. We then average the image across y to obtain an ensemble average $\langle U^*(-x)U(x)\rangle$. The y-averaging improves the signal-to-noise ratio of the interference curves by eliminating effects of beam inhomogeneities, such as the rings in Fig. 5 which are due to the 2π phase jumps in the SLMs of the interferometer. Mathematically, we have for the degree of coherence the expression

$$\mu(x, -x) = \frac{\int dy\, U^*(x, y)U(-x, y)}{\int dy\, \sqrt{S_1(x, y)S_2(x, y)}}, \tag{11}$$

where S_k, with $k = 1$ or 2, are the individual spectral densities of the two interferometer arms. Theoretically, the spectral degree of coherence μ measured by the interferometer is given by

$$\mu(x, -x) = \frac{\mu_{12} + \cos(2k_p x)}{1 + \mu_{12}\cos(2k_p x)}, \tag{12}$$

where $k_p = kd/(2f)$ is the spatial frequency of the far-field coherent modes. The measured spectral degrees of coherence according to Eq. (11) for selected values of μ_{12} are shown in Fig. 6. The value of k_p was chosen to be $2.0 \times 10^4\ \mathrm{m}^{-1}$. This ensures oversampling of the fringes by the CCD array with pixel size 4.4 μm. The maximum value of μ as measured by using Eq. (11) is not necessarily unity due to other sources of error. The SLM has 2π phase jumps which causes circular rings in the beam, hence the coherence value is not perfectly uniform across an individual coherent mode. Further sources of error are a small tilt phase difference between the two arms, beam inhomogenieties, a polarization mismatch in the two interferometer arms, and the laser not operating in a pure longitudinal mode. We therefore normalize the measured μ value by its largest value across x. We see very good agreement between the measured and theoretical curves. The coherence zeros predicted by the theory are accurately captured by the minima of the experimental curves. We conclude that the experiment unambiguously shows a drastic reduction of spatial coherence for highly correlated sources. Furthermore, such an anomalous decrease of coherence occurs not just in the context of radiation, but also in Mie scattering as we will next discuss.

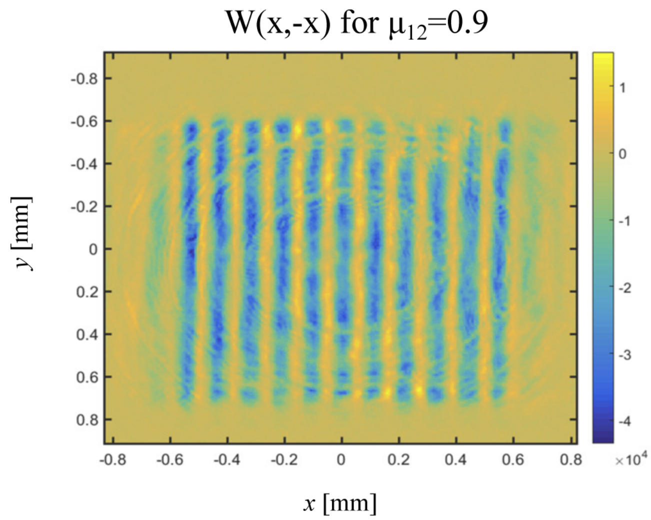

Fig. 5. The interference pattern representing the observed values of $\langle U^*(x,y)U(-x,y)\rangle$ for the case $\mu_{12} = 0.904$.

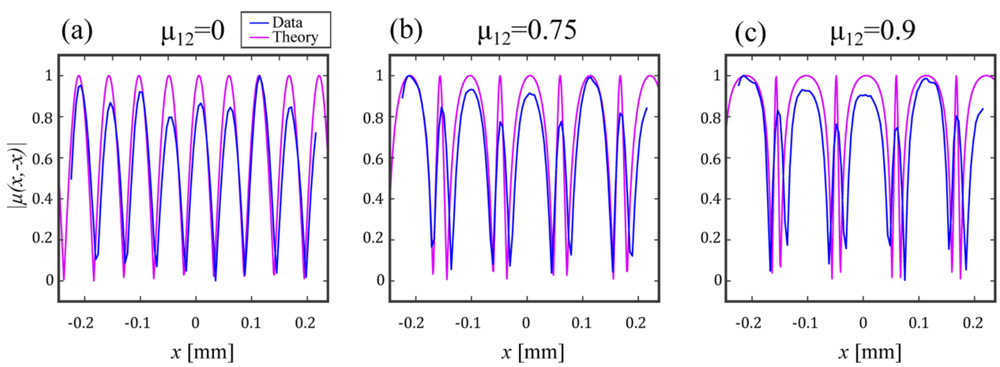

Fig. 6. Measured value of $|\mu(x,-x)|$ for (a) $\mu_{12} = 0$, (b) $\mu_{12} = 0.75$, and (c) $\mu = 0.9$. Blue lines show the measured data and purple lines show the expected theory curves.

4. Mie scattering

We next turn our attention to the scattering by a homogeneous sphere [13–15]. A formalism to study the far-zone coherence properties of the scattered Mie field (see Fig. 7) was recently presented in [16]. In that study an incident beam, propagating along the z axis, was assumed to have a uniform amplitude and a Gaussian spectral degree of coherence, i.e., $\mu^{(\mathrm{in})} = \exp[-(\rho_2 - \rho_1)^2/(2\sigma^2)]$. In this expression σ denotes the effective transverse coherence width, and $\rho = (x^2 + y^2)^{1/2}$. Three examples of the spectral degree of coherence in the far zone are shown in the bottom row of

Optics EXPRESS

Fig. 3. Panel (d) shows that even though the incident field is highly coherent, with a coherence width that is five times larger than the sphere radius a, there are pairs of directions for which $|\mu(\theta_1, \theta_2)|$ is strongly reduced. Even though the scattering process that produces this field is completely different from the radiation process that was discussed above, the similarities between panels a) and d) are striking. If the transverse coherence width of the incident field is reduced to $\sigma = 150\,\lambda = 1.5a$, the resulting spectral degree of coherence becomes as presented in panel e). In this case the coherence pattern is remarkably similar to its radiation counterpart panel b). Again a strong decrease of coherence is seen to occur. A third example is shown in f). This represents a very weakly coherent incident field with $\sigma = 20\lambda = 0.2a$. Once again the similarities, now with panel c), are compelling.

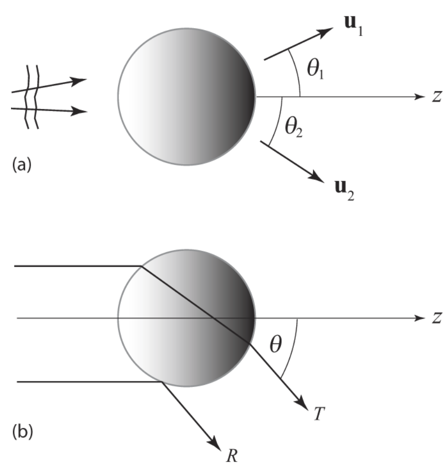

Fig. 7. Mie scattering by a homogeneous sphere with radius a and refractive index n. The center of the sphere is situated on the z axis. (a) If the incident field is spatially partially coherent, the field scattered in two directions $\mathbf{u}_1$ and $\mathbf{u}_2$, at angles θ_1 and θ_2 with the z axis, will be partially correlated. (b) The scattered field in a direction θ, mainly consisting of a transmitted ray with amplitude T, and a reflected ray with amplitude R.

The remarkable decrease of coherence in Fig. 3 occurs in two completely different contexts, namely radiation and scattering. What then explains the similarities between these two cases? On the one hand, the radiation of two partially correlated point sources, when considered in the far zone, leads to a simple model [Eq. (5)] that predicts that for certain pairs of directions the spectral degree of coherence will be increased, whereas for other directions it will be strongly decreased and can even become zero. On the other hand, the formalism that describes Mie scattering has the form of a sum of sometimes hundreds of Legendre polynomials (see Eq. (20) of Ref. [16]). The physical meaning of such a summation is much less clear. However, for spheres much larger than the wavelength a geometrical optics description is known to work quite well [17]. According to such a model, for many forward directions the main contribution to the scattered field is due to two rays, one that is reflected and one that is transmitted. Higher-order contributions, due to one or more internal reflections can, to first order, be neglected. This then reduces the Mie scattering process to the superposition of two parallel plane waves, with amplitudes R and T (see Fig. 7). If the scattering angle θ changes, the optical path difference between these two contributions changes, causing a continuous variation in the spectral degree of coherence. This explains why the drastic decrease of coherence that we found in the case of two highly-correlated radiating point sources also occurs in Mie scattering with highly coherent fields.

If the coherence length σ of the incident field is increased, the strong decrease of coherence of the scattered field is found to be remarkably persistent, but for gradually narrower angular

Optics EXPRESS

ranges. This is illustrated in Fig. 8. Even for coherence lengths much larger than the particle radius, near-zero values of $|\mu(\theta_1, 67°)|$ occur. It is only when $\sigma > 1000a$, that the scattered field is (almost) fully coherent.

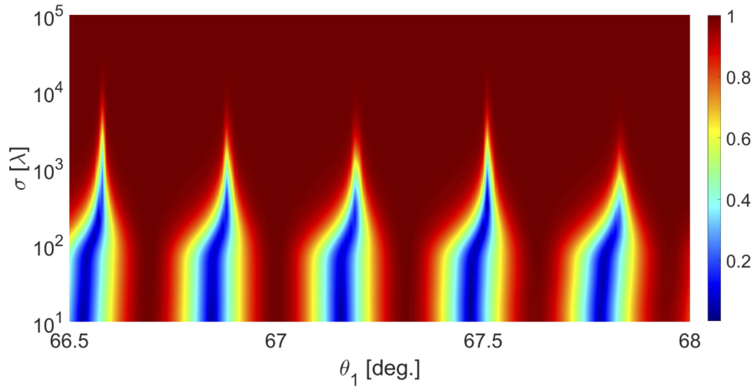

Fig. 8. Magnitude of the far-zone spectral degree of coherence $|\mu(\theta_1, 67°)|$ of a field scattered by a sphere with radius $a = 100\,\lambda$ and refractive index $n = 1.33$. The vertical axis shows the coherence length σ of the incident field (in free-space wavelengths), on a logarithmic scale.

The examples in the bottom row of Fig. 3 are for a large sphere for which the geometrical optics approach is reasonable, and depict an angular domain in which the amplitudes R and T are comparable. Also, the values of the coherence radius are chosen to yield a correlation between the reflected and the transmitted ray that is similar to the values of μ_{12} in the panels of the top row. More generally, it can be shown that a significant reduction of coherence still occurs even if the values of R and T are not comparable.

A somewhat hand-waiving explanation of our results is that the total field can be written as a sum of completely correlated parts and parts that are completely uncorrelated. In this picture, regions of low spectral density are where the correlated parts destructively interfere, leaving only the uncorrelated parts. This would then explain why such regions have a low mutual coherence. However, as was recently pointed out, such a decomposition is typically not unique [18].

5. Conclusion

The superposition of waves is central to quantum mechanics, acoustics and optics. We have examined, both theoretically and experimentally, the surprising phenomenon that, contrary to what might be expected, a field that starts out as highly coherent, can evolve into a field with near-zero coherence in certain directions. This effect occurs universally on wave superposition, as takes place in both radiation and scattering. This behavior can be considered the converse of that predicted by the van Cittert-Zernike theorem for highly uncorrelated sources, in which there is an increase in coherence on propagation.

The anomalous decrease of spatial coherence was demonstrated, both theoretically and experimentally, for a simple, highly-correlated radiation system. An almost fully coherent beam scattered by an extended Mie sphere was found to have a very similar behavior. We note that this is not a far-zone effect, it also occurs in the the proximity of sources and scatterers.

In practice, one often deals with two highly, but not perfectly, correlated sources, like two quantum dots that are driven resonantly by the same laser. The extreme decrease in coherence that we discussed should also occur in such cases. Because the state of coherence of a wave field determines its directionality and its ability to form interference fringes, this drastic decrease of coherence has consequences for optical design and imaging systems. Furthermore, we anticipate our discovery will have analogy in decoherence processes for evolving quantum systems [19].

Appendix

A. Derivation of Eq. (5)

The spectral density at an observation point P_1 is given by Eq. (2), i.e.,

$$S(P_1,\omega) = \frac{S_1(\omega)}{R_{11}^2} + \frac{S_2(\omega)}{R_{21}^2} + \frac{2\sqrt{S_1(\omega)S_2(\omega)}}{R_{11}R_{21}}\mathrm{Re}\left[\mu_{12}(\omega)e^{\mathrm{i}kn(R_{21}-R_{11})}\right]. \tag{13}$$

To simplify our notation we suppress the ω dependence of the various quantities from now on, and we denote the observation points in the plane $z = z_0$ by their angle θ with the positive z axis. We consider the case that $S_1 = S_2 = S$, $n = 1$, and $\mu_{12} \in \mathbb{R}$. In the far zone we have the approximations

$$R_{11} \approx R_1 - (d/2)\sin\theta_1. \tag{14}$$

$$R_{21} \approx R_1 + (d/2)\sin\theta_1. \tag{15}$$

$$R_{12} \approx R_2 - (d/2)\sin\theta_2. \tag{16}$$

$$R_{22} \approx R_2 + (d/2)\sin\theta_2. \tag{17}$$

$$1/R_{ij}^2 \approx 1/R^2, \quad \text{for } i,j = 1,2. \tag{18}$$

On making use of these expression in Eq. (13) it is readily found that

$$S(\theta_1) = \frac{2S}{R^2}\left[1 + \mu_{12}\cos(kd\sin\theta_1)\right], \tag{19}$$

and, in a completely similar way, that

$$S(\theta_2) = \frac{2S}{R^2}\left[1 + \mu_{12}\cos(kd\sin\theta_2)\right]. \tag{20}$$

The spectral degree of coherence at two points P_1 and P_2 is defined as

$$\mu(\theta_1,\theta_2) = \frac{\langle U^*(\theta_1)U(\theta_2)\rangle}{\sqrt{S(\theta_1)S(\theta_2)}}. \tag{21}$$

Using the expressions (19) and (20) for the spectral density and the approximations that were used in their derivation, it is straightforward to show that

$$\begin{aligned}\mu(\theta_1,\theta_2) = e^{\mathrm{i}k(R_2-R_1)}\,&\{\cos[k(d/2)(\sin\theta_1 - \sin\theta_2)] \\ &+\mu_{12}\cos[k(d/2)(\sin\theta_1 + \sin\theta_2)]\} \\ &\times[1 + \mu_{12}\cos(kd\sin\theta_1)]^{-1/2}[1 + \mu_{12}\cos(kd\sin\theta_2)]^{-1/2}.\end{aligned} \tag{22}$$

We next choose $\theta_2 = 0$, and obtain

$$|\mu(\theta_1,0)|^2 = \frac{(1+\mu_{12})\cos^2[k(d/2)\sin\theta_1]}{1+\mu_{12}\cos(kd\sin\theta_1)}, \tag{23}$$

which is Eq. (5).

Optics EXPRESS

B. Two limiting cases

For the sake of completeness we consider the two limits of complete incoherence ($\mu_{12} = 0$) and full coherence ($\mu_{12} = 1$). In the first case Eq. (5) reduces to

$$\mu(\theta_1, 0) = \cos[kn(d/2)\sin\theta_1], \quad (\mu_{12} = 0). \tag{24}$$

On varying the angle θ_1 the spectral degree of coherence is seen to oscillate between zero and plus or minus one. This is exactly the behavior predicted by the van Cittert-Zernike theorem [2].

In the case of full coherence we find that

$$|\mu(\theta_1, 0)|^2 = \frac{2\cos^2[k(d/2)\sin\theta_1]}{1+\cos(kd\sin\theta_1)} = \frac{2\cos^2[k(d/2)\sin\theta_1]}{2\cos^2[k(d/2)\sin\theta_1]}, \quad (\mu_{12} = 1). \tag{25}$$

This equals 1 execept when $kd\sin\theta_1 = \pm(m+1)\pi$, with $m = 0, 1, 2, \ldots$, in which case the expression is indeterminate. Using l'Hôpital's rule we find that $|\mu(\theta_1, 0)| = 1$ for those values of θ_1 also, as was expected.

C. Coherent mode decomposition

For the case of two point sources the field in the source plane may be approximated by the expression

$$U(x, z=0) = A_1\delta(x+d/2) + A_2\delta(x-d/2) \tag{26}$$

where A_1 and A_2 denote an amplitude. We take $\langle|A_1|^2\rangle = \langle|A_2|^2\rangle = A^2$, and $\langle A_1^* A_2\rangle = \mu_{12}A^2$. The CSD is then

$$\begin{aligned} W(x_1, x_2, z=0) &\equiv \langle U^*(x_1, 0)U(x_2, 0)\rangle \\ &= A^2\delta(x_1+d/2)\delta(x_2+d/2) + A^2\delta(x_1-d/2)\delta(x_2-d/2) \end{aligned} \tag{27}$$

$$+A^2\mu_{12}\delta(x_1+d/2)\delta(x_2-d/2) + A^2\mu_{12}\delta(x_1-d/2)\delta(x_2+d/2), \tag{28}$$

with the spectral degree of coherence μ_{12} assumed to be real. The CSD can be represented via the CMD (Cf. Equation (7)) as

$$W(x_1, x_2, z=0) = \sum_m \lambda_m \phi_m^*(x_1)\phi_m(x_2), \tag{29}$$

where the coherent modes $\phi_m(x)$ are orthogonal and satisfy a homogeneous Fredholm equation of the second kind with the kernel $W(x_1, x_2)$. It can be shown by construction that there are two coherent modes in this case, namely

$$\phi_1(x) = C\left[\delta(x+d/2) + \delta(x-d/2)\right], \tag{30}$$

$$\phi_2(x) = C\left[\delta(x+d/2) - \delta(x-d/2)\right], \tag{31}$$

with C a constant. On substituting these expressions into Eq. (29) we obtain

$$\begin{aligned} W(x_1, x_2, z=0) = {} & |C|^2(\lambda_1+\lambda_2)\left[\delta(x_1+d/2)\delta(x_2+d/2)\right] \\ & + |C|^2(\lambda_1+\lambda_2)\left[\delta(x_1-d/2)\delta(x_2-d/2)\right] \\ & + |C|^2(\lambda_1-\lambda_2)\left[\delta(x_1+d/2)\delta(x_2-d/2)\right] \\ & + |C|^2(\lambda_1-\lambda_2)\left[\delta(x_1-d/2)\delta(x_2+d/2)\right]. \end{aligned} \tag{32}$$

Comparing Eqs. (28) and (32) it is found that if

$$A^2 = |C|^2(\lambda_1+\lambda_2), \tag{33}$$

Optics EXPRESS

$$A^2\mu_{12} = |C|^2(\lambda_1 - \lambda_2), \tag{34}$$

then Eqs. (28) and (32) will be equal, and hence

$$\mu_{12} = \frac{\lambda_1 - \lambda_2}{\lambda_1 + \lambda_2}, \tag{35}$$

which is Eq. (8). It can be seen that the coherent modes given by Eqs. (30) and (31) are indeed orthogonal and satisfy the associated Fredholm integral equation. Also note that only in the completely incoherent limit of $\mu_{12} = 0$ can the CSD be alternatively decomposed into $\phi_1(x) = \delta(x + d/2)$ and $\phi_2(x) = \delta(x - d/2)$, which is a manifestation of the non-uniqueness of the CMD.

D. Derivation of Eq. (12)

As described in the *Experimental Verification* section of the main text, the two source coherent modes get Fourier transformed by a lens to generate their far-zone forms. This implies that the fields of the two coherent modes in the back focal plane ($z = 2f$) are [8]

$$\phi_1(x, z = 2f) = 2A\cos(k_p x), \tag{36}$$

$$\phi_2(x, z = 2f) = 2iA\sin(k_p x), \tag{37}$$

with A an arbitrary amplitude and $k_p = kd/(2f)$. By using Eq. (7) one finds for the cross-spectral density in the focal plane the expression

$$W(x_1, x_2, z = 2f) = \lambda_1 4A^2\cos(k_p x_1)\cos(k_p x_2) + \lambda_2 4A^2\sin(k_p x_1)\sin(k_p x_2). \tag{38}$$

If we set $x_1 = x$ and $x_2 = -x$ and recall the definition (3) of the degree of coherence, then it is readily derived that

$$\mu(x, -x, z = 2f) = \frac{\lambda_1\cos^2(k_p x) - \lambda_2\sin^2(k_p x)}{\lambda_1\cos^2(k_p x) + \lambda_2\sin^2(k_p x)}. \tag{39}$$

Using Eq. (35) this can be written in the form of Eq. (12), i.e.

$$\begin{aligned}\mu(x, -x, z = 2f) &= \frac{(1 + \mu_{12})\cos^2(k_p x) - (1 - \mu_{12})\sin^2(k_p x)}{(1 + \mu_{12})\cos^2(k_p x) + (1 - \mu_{12})\sin^2(k_p x)},\\ &= \frac{\mu_{12} + \cos(2k_p x)}{1 + \mu_{12}\cos(2k_p x)}.\end{aligned} \tag{40}$$

Funding. Defense Advanced Research Projects Agency (YFA D19AP00042).

Acknowledgments. S. A. W. acknowledges Prof. J. R. Fienup for useful discussions.

Disclosures. The authors declare that there are no conflicts of interest related to this article.

Data availability. Data for Figs. 5 and 6 are available from the authors upon reasonable request.

References

1. E. Wolf, *Introduction to the Theory of Coherence and Polarization of Light* (Cambridge University Press, Cambridge, 2007).
2. L. Mandel and E. Wolf, *Optical Coherence and Quantum Optics* (Cambridge University Press, Cambridge, 1995).
3. G. S. Agarwal, G. Gbur, and E. Wolf, "Coherence properties of sunlight," Opt. Lett. **29**(5), 459–461 (2004).
4. H. Mashaal, A. Goldstein, D. Feuermann, and J. M. Gordon, "First direct measurement of the spatial coherence of sunlight," Opt. Lett. **37**(17), 3516–3518 (2012).
5. S. Divitt and L. Novotny, "Spatial coherence of sunlight and its implications for light management in photovoltaics," Optica **2**(2), 95–103 (2015).
6. T. D. Visser and R. W. Schoonover, "A cascade of singular field patterns in Young's interference experiment," Opt. Commun. **281**(1), 1–6 (2008).

Optics EXPRESS

7. E. Wolf, "New spectral representation of random sources and of the partially coherent fields that they generate," Opt. Commun. **38**(1), 3–6 (1981).
8. J. W. Goodman, *Introduction to Fourier Optics*, 2nd ed. (McGraw Hill, New York, 1996).
9. B. Rodenburg, M. Mirhosseini, O. S. Magana-Loaiza, and R. W. Boyd, "Experimental generation of an optical field with arbitrary spatial coherence properties," J. Opt. Soc. Am. B **31**(6), A51–A55 (2014).
10. X. Chen, J. Li, S. M. H. Rafsanjani, and O. Korotkova, "Synthesis of I_m-Bessel correlated beams via coherent modes," Opt. Lett. **43**(15), 3590–3593 (2018).
11. V. Arrizón, U. Ruiz, R. Carrada, and L. A. González, "Pixelated phase computer holograms for the accurate encoding of scalar complex fields," J. Opt. Soc. Am. A **24**(11), 3500–3507 (2007).
12. T. Malhotra, W. E. Farriss, J. Hassett, A. F. Abouraddy, J. R. Fienup, and A. N. Vamivakas, "Interferometric spatial mode analyzer with a bucket detector," Opt. Express **26**(7), 8719–8728 (2018).
13. G. Mie, "Beiträge zur Optik trüber Medien, speziell kolloidaler Metallösungen," Ann. Phys. **330**(3), 377–445 (1908).
14. M. Born and E. Wolf, *Principles of Optics*, 7th ed (Cambridge University Press, Cambridge, 1995).
15. T. van Dijk, D. G. Fischer, T. D. Visser, and E. Wolf, "Effects of spatial coherence on the angular distribution of radiant intensity generated by scattering on a sphere," Phys. Rev. Lett. **104**(17), 173902 (2010).
16. H. F. Schouten, D. G. Fischer, and T. D. Visser, "Coherence modification and phase singularities on scattering by a sphere: Mie formulation," J. Opt. Soc. Am. A **36**(12), 2005–2010 (2019).
17. J. A. Adam, "The mathematical physics of rainbows and glories," Phys. Rep. **356**(4-5), 229–365 (2002).
18. A. Halder, J. Turunen, and A. T. Friberg, "Correlated and uncorrelated parts of scalar fields in two-beam optical interferometry," Opt. Lett. **46**(2), 396–399 (2021).
19. S. Haroche and J. M. Raimond, *Exploring the Quantum* (Oxford University Press, Oxford, 2006).